Int. J. Solids Structures Vol. 30, No. 23, pp. 3261–3280, 1993
Printed in Great Britain

0020–7683/93 $6.00+ .00
Pergamon Press Ltd

FINITE ELEMENT ANALYSIS OF THE BEHAVIOR OF SHAPE MEMORY ALLOYS AND THEIR APPLICATIONS

L. C. BRINSON† and R. LAMMERING
Deutsche Forschungsanstalt für Luft- und Raumfahrt, Institut für Aeroelastik, Bunsenstraße 10, 3400 Göttingen, Germany

(*Received* 8 *September* 1992; *in revised form* 17 *May* 1993)

Abstract—A nonlinear finite element procedure is developed which incorporates a thermodynamically derived constitutive law for shape memory alloy material behavior. The constitutive equations include the necessary internal variables to account for the material transformations and are utilized in a one-dimensional finite element procedure that captures the unique shape memory alloy responses of pseudoelasticity and of the shape memory effect at all temperatures, stress levels and loading conditions. Detailed material properties for the alloy used are necessary for the analysis. The solution of the geometrically and physically nonlinear problem is achieved by application of a Newton's method in which a sequence of linear problems is numerically solved. Due to consistent linearization, a quadratic rate of convergence is obtained.

Several test cases are presented to illustrate the potential of the finite element procedure. Cases simulating the stress–strain behavior of a bar of shape memory alloy under simple uniaxial loading as well as restrained recovery responses at different temperatures compare well with experimental and analytical results. Two further generalized applications are examined: the use of a shape memory alloy ring as a pipe connector and eigenfrequency tuning of a composite beam with embedded shape memory wires. The results of these analyses correlate well with analytical results and the methodology for use of the finite element procedure in general cases is demonstrated. The finite element procedure is thus shown to be a powerful tool for studying various applications of shape memory alloys.

INTRODUCTION

Shape memory alloys (SMA) materials have the unusual material property of being able to sustain and recover large strains (of the order of 10%) without inducing irreversible plastic deformation and to "remember" a previous configuration and return to it with a temperature change. These interesting material characteristics arise due to distinctive internal crystalline transformations with temperature and applied stress (Delaey *et al.*, 1974; Perkins *et al.*, 1976; Funakubo, 1987; Wayman and Duerig, 1990). The growing global interest in smart material and smart structure technology in particular has prompted an increasing number of investigations of SMAs in the past decade. The result of this research has been increasingly detailed information regarding the crystalline structure of SMA materials, a greater understanding of macroscopic SMA material behavior, the development of new alloys and processing techniques, and a dramatic increase in the number of applications studied, which now span a wide range of products and devices. The most established commercial application of SMAs, that of connectors for hydraulic tubing in aircraft, is currently being overshadowed by the incorporation of SMAs into critical roles in a large array of applications including active vibration control of structures, heat engines, orthodontic wire and automatic switches in household appliances (Banks and Weres, 1976; Funakubo, 1987; Rogers *et al.*, 1989; Falcioni, 1992).

One advantage of shape memory alloys over other types of mechanical or electrical devices is that their physical configuration can be easily, precisely and repeatedly controlled by often small temperature changes. In some applications, where temperature change is in itself the motivation for movement of a mechanical device, the SMAs can be designed such that no power source is needed to activate their motion. In other cases, a single or series of SMA wires can easily and inexpensively be given a small temperature change which initiates

†Current address: Department of Mechanical Engineering, Northwestern University, 2145 N. Sheridan Road, Evanston, IL 60208, U.S.A.

a phase transformation and consequently results in the desired motion and/or stress. Their ability to achieve large strains near instantaneously enables the design of structures capable of extremely large, recoverable deflections. In addition, shape memory alloys are relatively lightweight, biocompatible, easy to manufacture and have a high force to weight ratio (Wayman, 1980).

Given the variety of potential uses for SMAs and the high interest in developing new applications, the ability to accurately model and analyse structures containing SMA components via a finite element procedure is extremely attractive. The authors are unaware of any existing finite element analyses capable of addressing shape memory behavior. The incorporation of the SMA finite element procedure into the design stages of new products could reduce development times and costs dramatically. Since the properties of a particular alloy can be easily and drastically altered in the manufacturing process, the properties of the SMA component in a given design can be varied systematically in the finite element analysis before production. This optimization procedure will enable use of shape memory alloy components with specifically tailored properties that will realize their full potential in each individual application.

Due to the nature of the internal crystalline transformations, shape memory alloys are best utilized in an essentially one-dimensional manner, that is, in applications in which the primary stress and strain directions for the SMA component lie always on a single axis. Consequently, the current research and available data on SMAs is primarily one-dimensional in nature and here a one-dimensional finite element procedure is developed. The study of SMA applications with the finite element analysis is not so strictly limited: only the function of the SMA component itself must be predominantly one-dimensional. Thus, the finite element procedure results in models that are highly accurate for many systems incorporating SMAs.

In this work, first the physical basis of SMA behavior is outlined and a general one-dimensional constitutive law representing this behavior is reviewed. The weak form of the momentum balance for static boundary value problems and its linearization are summarized and then the derivation of the tangent operator in a rigorous linearization of the SMA constitutive law is shown. This method preserves a quadratic rate of convergence in the iterative solution algorithm which is based on Newton's method. A discussion of the possibilities and requirements of the finite element procedure follows and several simple examples of the response of the shape memory material alone are presented, the results of which correlate well with experimental and analytical results. A demonstration of a more complex application, a SMA pipe connector, is also given. Finally, a method by which the one-dimensional SMA finite element for shape memory alloy components can be linked to two dimensional structural problems is demonstrated and discussed via an example of a composite beam with embedded SMA wires. In all cases, experimental, analytical and calculated results are in good agreement.

REVIEW OF SMA CONSTITUTIVE BEHAVIOR

In this section the physical processes behind shape memory behavior are sketched briefly. The major effects are explained in an attempt to give a framework, motivation and context for the remainder of the paper, but for more complete discourse regarding the topics covered, please refer to the relevant work cited.

The special mechanical properties of shape memory alloys depend upon internal crystalline transformations as functions of stress, temperature and history of the material. At high temperatures under stress-free conditions, a SMA exists in the parent phase (austenite) and when cooled the material undergoes a transformation to the low temperature phase (martensite). In the stress-free state a SMA material can be considered to have four transition temperatures, designated as M_f, M_s, A_s, A_f: martensite finish, martensite start, austenite start, austenite finish. The phase changes occur between the respective start and finish temperatures and for clarity in this paper we restrict ourselves to examining the situation in which $M_f < M_s < A_s < A_f$. Note that a change of temperature, T, within the range $M_s < T < A_s$ induces no phase changes and both martensite and austenite can coexist

within $M_f < T < A_f$. The formation of the martensite phase from the parent phase under zero stress is a self-accommodating transformation in which multiple twins and variants of martensite are formed and there is no volume change or global strain. The martensite variants formed are all crystallographically and energetically equivalent in the absence of stress, differing only in orientation, and are distributed evenly throughout the material. The ability of SMAs to achieve large reversible strains derives directly from the self-accommodating nature of this transformation (Warlimont *et al.*, 1974; Funakubo, 1987; Wayman and Duerig, 1990).

When unidirectional stress is applied to the SMA material, there is a critical value, dependent upon temperature, at which the martensite variants begin a "detwinning" process that results ultimately in the material consisting of a single variant of martensite aligned with the axis of loading. Additionally, for material in the austenite phase prior to loading, there is likewise a critical stress value, dependent upon temperature, at which the austenite undergoes a crystalline transformation to martensite and in fact, because of the presence of stress, to a single variant of detwinned martensite. In the transformation process to detwinned martensite with the application of load, the stress raises only slightly and a large, apparently plastic strain is achieved. If the material temperature is above A_f, this large strain will be recovered by unloading in a characteristic hysteresis loop since the martensite is unstable at such temperatures without stress; this overall loading and unloading effect is termed pseudoelasticity. If the material temperature is below A_s, a large residual strain remains after unloading, but may be recovered by heating the material above the austenite finish temperature; this behavior is generally termed the shape memory effect and a schematic of the detwinning process is shown in Fig. 1. (Also see Fig. 2, illustrating the critical stresses as functions of temperature, and Fig. 3 in the Discussion Section which depicts typical stress–strain curves of SMA materials at various temperatures.)

Constitutive relations

This past decade has seen the development of a number of approaches and techniques for describing shape memory alloy constitutive behavior (Falk, 1980, 1983; Tanaka, 1986; McNichols and Cory, 1987; Achenbach, 1989; Liang and Rogers, 1990; Brinson, 1992). For these methods to be readily useful in numerical analysis, the material behavior must not only be accurately described in mathematical form but also in a form that is amenable to its inclusion in numerical procedures. For this study the constitutive relations developed by Brinson (1992, 1993), based on previous work by Liang (Liang, 1990; Liang and Rogers, 1990) and Tanaka (Tanaka and Nagaki, 1982; Tanaka and Iwasaki, 1985; Tanaka, 1986) are utilized. This constitutive description is derived on a thermomechanical basis, has a relatively simple mathematical expression and includes only quantifiable engineering variables and material parameters in its expression. The latter is important since a major drawback to many of the constitutive relations previously developed is that they directly

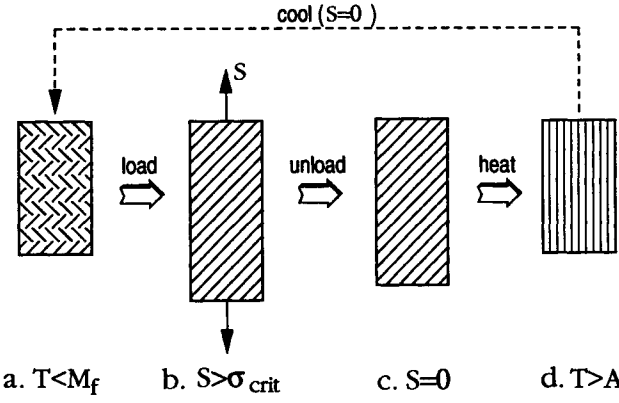

Fig. 1. Schematic of detwinning and phase transformation. In (a) twinned martensite, in (b) and (c) detwinned martensite, in (d) austenite.

include variables that are not easily quantified for standard solid mechanics applications, such as free energy.

Here we briefly review the development of the constitutive law which will be used in the finite element analysis. Based upon energy balance equations, a basic differential form of the SMA constitutive law can be derived (Tanaka, 1986; Brinson, 1993) as

$$dS = D(E, \xi, T)\,dE + \Omega(E, \xi, T)\,d\xi_s + \Theta(E, \xi, T)\,dT, \tag{1}$$

where S is the second Piola–Kirchhoff stress, E is the Green strain and ξ is an internal variable representing the stage of the transformation. The function $D(E, \xi, T)$ represents the modulus of the SMA material, $\Omega(E, \xi, T)$ is considered the "transformation tensor", and $\Theta(E, \xi, T)$ is related to the thermal coefficient of expansion for the SMA material. The martensite fraction, ξ, is further defined by

$$\xi = \xi_S + \xi_T, \tag{2}$$

where ξ_T represents the fraction of the material that is purely temperature-induced martensite with multiple variants and ξ_S denotes the fraction of the material that has been transformed, or oriented, by stress into a *single* martensite variant.

In general, the Young's modulus of a SMA is a function of the martensite fraction of the material, with the austenitic modulus being approximately three times larger than the martensitic modulus. To account for this functionality, here the modulus is chosen to be a simple linear function of the martensite fraction

$$D(E, \xi, T) = D(\xi) = D_a + \xi(D_m - D_a), \tag{3}$$

where D_m is the modulus value for the SMA as 100% martensite (twinned or detwinned) and D_a is the modulus value for the SMA as 100% austenite. Regarding the transformation tensor, in a constitutive derivation of (1) with constant material functions, a relationship between the modulus and Ω is enforced by applying the material restriction of maximum residual strain. The maximum residual strain, ε_L, of a SMA is a material constant and can be obtained experimentally by converting all the material to detwinned martensite (to $\xi_S = 1$) and then unloading at a temperature less than A_s. Using the relationship for constant material functions, it can also be shown (Brinson, 1993) that the transformation tensor as a function of ξ is intimately related to the modulus function and can be expressed as

$$\Omega(\xi) = -\varepsilon_L D(\xi). \tag{4}$$

Thus the transformation tensor is not an independent material constant. The material function $\Theta(E, \xi, T)$ is generally assumed to remain constant due to its necessarily relatively small value [five orders of magnitude less than $D(\xi)$].

Given the assumption that the material parameters are linear in ξ, reasonable for a majority of shape memory alloys, the constitutive law can be derived to be

$$S - S_0 = D(\xi)E - D(\xi_0)E_0 + \Omega(\xi)\xi_S - \Omega(\xi_0)\xi_{S0} + \Theta(T - T_0), \tag{5}$$

where $(S_0, E_0, \xi_0, \xi_{S0}, T_0)$ represent the initial state (or initial conditions) of the material. Note that although eqn (5) is valid for a wide range of shape memory alloys, if the material properties for a particular SMA are known to be more general functions of the martensite fraction or are functions of the other independent variables, then eqn (5) must be rederived from the basic differential form using the methodology previously discussed (Brinson, 1993).

Transformation kinetics

In addition to the direct expression of the constitutive law, since the martensite fraction depends on stress and temperature, a set of equations describing this relationship must be

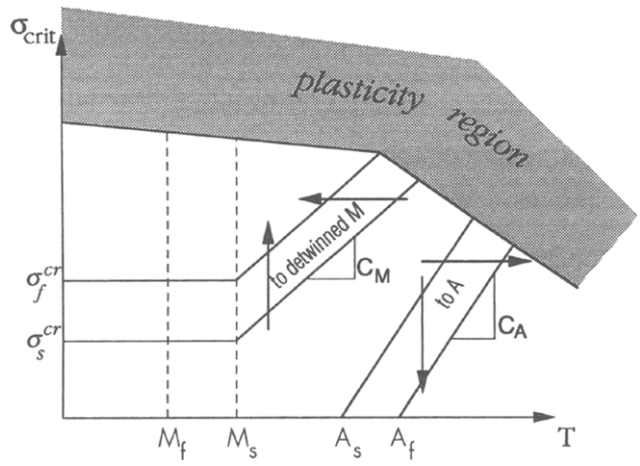

Fig. 2. Critical stresses for transformation or martensite twin conversion as functions of temperature. Plasticity region indicated.

coupled with eqn (5) in order to have a complete set of governing equations for shape memory alloy behavior. The phase transformation between austenite and martensite is controlled by chemical free energy as the driving force and a thorough development of the theory of transformation kinetics can be found in the literature (Warlimont *et al.*, 1974; Funakubo, 1987) and is not presented here. An empirically based cosine model to represent the martensite fraction as a function of stress and temperature during transformation has been developed (Liang and Rogers, 1990) and then further modified to be compatible with eqns (2) and (5) and to capture shape memory behavior at all temperatures (Brinson, 1993). For completeness, these equations are repeated here. In conjunction with Fig. 2, illustrating the critical transformation stress for crystalline transformations, expressions for the martensite fraction are as follows:

Conversion to detwinned martensite

for $\mathbf{T} > \mathbf{M}_s$ and $\sigma_s^{cr} + C_M(T - M_s) < S < \sigma_f^{cr} + C_M(T - M_s)$:

$$\xi_S = \frac{1-\xi_{S0}}{2}\cos\left\{\frac{\pi}{\sigma_s^{cr}-\sigma_f^{cr}}(S-\sigma_f^{cr}-C_M(T-M_s))\right\}+\frac{1+\xi_{S0}}{2}, \tag{6a}$$

$$\xi_T = \xi_{T0} - \frac{\xi_{T0}}{1-\xi_{S0}}(\xi_S - \xi_{S0}), \tag{6b}$$

for $\mathbf{T} < \mathbf{M}_s$ and $\sigma_s^{cr} < S < \sigma_f^{cr}$:

$$\xi_S = \frac{1-\xi_{S0}}{2}\cos\left\{\frac{\pi}{\sigma_s^{cr}-\sigma_f^{cr}}(S-\sigma_f^{cr})\right\}+\frac{1+\xi_{S0}}{2}, \tag{6c}$$

$$\xi_T = \xi_{T0} - \frac{\xi_{T0}}{1-\xi_{S0}}(\xi_S - \xi_{S0}) + \Delta_{T\xi}, \tag{6d}$$

where,

if $M_f < T < M_s$ and $T < T_0$,

$$\Delta_{T\xi} = \frac{1-\xi_{T0}}{2}[\cos(a_M(T-M_f))+1]$$

else,

$$\Delta_{T\xi} = 0. \tag{6e}$$

Conversion to austenite

For $T > A_s$ and $C_A(T-A_f) < S < C_A(T-A_s)$:

$$\xi = \frac{\xi_0}{2}\left\{\cos\left[a_A\left(T-A_s-\frac{S}{C_A}\right)\right]+1\right\}, \tag{7a}$$

$$\xi_S = \xi_{S0} - \frac{\xi_{S0}}{\xi_0}(\xi_0-\xi), \tag{7b}$$

$$\xi_T = \xi_{T0} - \frac{\xi_{T0}}{\xi_0}(\xi_0-\xi). \tag{7c}$$

The parameters a_M and a_A are defined by

$$a_M = \frac{\pi}{M_s-M_f}, \quad a_A = \frac{\pi}{A_f-A_s}. \tag{8}$$

The constants C_M and C_A are material properties which describe the relationship of temperature and the critical stress to induce transformation, σ_{crit}, as illustrated in Fig. 2. Note that above the M_s temperature, the value of the stress necessary to achieve transformation to detwinned martensite (as well as the stress below which martensite transforms to austenite) increases with temperature as is physically intuitive. The critical stress values below M_s are taken to be constant in this model and are denoted by σ_s^{cr} and σ_f^{cr} for the critical stresses at the start and finish of the conversion of the martensitic variants. Sufficient experimental evidence is not available to distinguish between the critical stresses for transformation of austenite to martensite and the critical stresses for conversion of martensite twins at a given temperature. Since the stress–strain curves of shape memory alloys do not generally exhibit two distinct transformation regions, it is reasonable to assume that the transformation and conversion stresses are identical for the purposes of this paper.

ANALYTICAL AND NUMERICAL FORMULATION

The derivation and description of the equations necessary for the numerical study of SMAs is divided into three sections. The first section presents the linearization of the weak form of the momentum balance equation as applied generally to three-dimensional solid mechanics problems, leaving the constitutive behavior as yet unspecified. In the second section the consistent linearization of the shape memory alloy constitutive behavior represented by eqns (5)–(7) is performed one-dimensionally, but allowing the material to retain orientation in three-dimensional space. The third section describes the actual implementation of the previous linearization techniques in a finite element procedure for three-dimensional truss elements of shape memory alloys.

Linearization of the weak form of momentum balance

In addition to the constitutive relations, the momentum balance equations and suitable boundary conditions must be considered for the eventual numerical study of shape memory alloy behavior. Using the principles of virtual displacement, a weak formulation of the resulting boundary value problem in the reference configuration can be given by

$$G(\mathbf{x},\eta) = \int_V \mathbf{P}\cdot\mathrm{Grad}\,\eta\,\mathrm{d}V - \int_V \rho_0(\mathbf{b}-\ddot{\mathbf{x}})\cdot\eta\,\mathrm{d}V - \int_A \bar{\mathbf{t}}\cdot\eta\,\mathrm{d}A = 0, \tag{9}$$

where $\mathbf{x}$ is the current position vector in a rectangular Cartesian coordinate system, $\mathbf{P}$ denotes the first Piola–Kirchhoff stress tensor and η the usual vector of virtual displacements

for a body of volume V. The density of the body in the reference configuration is ρ_0, $\rho_0\mathbf{b}$ are body forces and $\rho_0\ddot{\mathbf{x}}$ the inertial forces per unit volume. External conservative forces $\bar{\mathbf{t}}$ are applied to the surface area of the body, A.

Due to the implementation of the SMA constitutive law, and because of the large strains achieved in normal use of SMAs, eqn (9) becomes nonlinear in the displacements. An iterative solution technique based on Newton's method is used in order to preserve quadratic rate of convergence. This algorithm makes use of the expansion of the nonlinear equations in a Taylor series at the location of a given approximation. The procedure for linearizing the equations of continuum mechanics is comprehensively described in Marsden and Hughes (1983) and Hughes and Pister (1978). At a known configuration, $\bar{\mathbf{x}}$, the linearization of the nonlinear function, $G(\mathbf{x}, \eta)$, is given by

$$G(\mathbf{x}, \eta) \cong G(\bar{\mathbf{x}}, \eta) + \mathscr{D}\{\bar{G}\} \cdot \mathbf{u}, \tag{10}$$

where $\mathbf{x} = \bar{\mathbf{x}} + \mathbf{u}$ and the operator $\mathscr{D}\{\bar{G}\} \cdot \mathbf{u}$ is the derivative of G at $\bar{\mathbf{x}}$ in the direction of $\mathbf{u}$ and is obtained by

$$\mathscr{D}\{\bar{G}\} \cdot \mathbf{u} = \frac{\partial G(\bar{\mathbf{x}}, \eta)}{\partial \mathbf{x}} \cdot \mathbf{u} = \frac{\mathrm{d}}{\mathrm{d}\varepsilon}\{G(\bar{\mathbf{x}} + \varepsilon\mathbf{u}, \eta)\}|_{\varepsilon=0}. \tag{11}$$

Rigorous linearization of the weak formulation of the momentum balance equation results in (Wriggers, 1988)

$$G(\mathbf{x}, \eta) = G(\bar{\mathbf{x}}, \eta) + \int_V \mathrm{Grad}\, \mathbf{u}\mathbf{S}(\bar{\mathbf{x}}) \cdot \mathrm{Grad}\, \eta \, \mathrm{d}V + \int_V \mathbf{F}(\bar{\mathbf{x}}, \eta)[\mathscr{D}\{\mathbf{S}(\bar{\mathbf{x}})\} \cdot \mathbf{u}] \cdot \mathrm{Grad}\, \eta \, \mathrm{d}V. \tag{12}$$

Here, $\mathbf{F}$ denotes the deformation gradient and $\mathbf{S}$ is again the second Piola–Kirchhoff stress. The linearization of $\mathbf{S}$ is calculated in the next section with respect to the constitutive relations of shape memory alloys. In a finite element formulation, the first integral expression of eqn (12) results in the initial stress matrix, the second includes the linear stiffness matrix and the initial displacement matrix. Newton's algorithm is obtained when eqn (10) is set to zero and the deformation increment is calculated by

$$\mathscr{D}\{G(\bar{\mathbf{x}}, \eta)\} \cdot \mathbf{u} = -G(\bar{\mathbf{x}}, \eta). \tag{13}$$

Linearization of the SMA constitutive law

The linearization procedure applied to the momentum balance equation in the previous section is now used for the calculation of the linearized SMA constitutive law. With regard to the truss application, the generalized three-dimensional notation is now reduced to one-dimension, the x-direction representing the material direction, with the allowance that the one-dimensional material body has a location and orientation in three-dimensional space. Splitting eqn (5) into constant and nonconstant terms, one obtains

$$S = D(\xi)[E - \varepsilon_L \xi_S] + K_0, \tag{14}$$

where the term K_0 contains the lumped contributions of the constants,

$$K_0 = S_0 - D(\xi_0)E_0 - \Omega(\xi_0)\xi_{S0} + \Theta(T - T_0). \tag{15}$$

Note that the temperature is assumed to be constant for each element in the material in this formulation and heat transfer effects are not considered. Given the expression (14) for the constitutive relation, the substitution can be made directly in eqn (12) in the term for the directional derivative of the second Piola–Kirchhoff stress. Up until this point, there

need be no change in the derivation procedure. Examining this derivative term alone, one obtains

$$\mathscr{D}\{S(\bar{\mathbf{x}})\}\cdot\mathbf{u} = \frac{\mathrm{d}}{\mathrm{d}\varepsilon}\{S(\bar{x}+\varepsilon u)\}|_{\varepsilon=0}$$

$$= \frac{\mathrm{d}}{\mathrm{d}\varepsilon}\{D(\xi(\bar{x}+\varepsilon u))\{E(\bar{x}+\varepsilon u)-\varepsilon_{\mathrm{L}}\xi_{\mathrm{S}}(\bar{x}+\varepsilon u)\}+K_0\}|_{\varepsilon=0}. \tag{16}$$

Applying the chain rule and simplifying results in

$$\frac{\mathrm{d}}{\mathrm{d}\varepsilon}\{S(\bar{x}+\varepsilon u)\}|_{\varepsilon=0} = \{E(\bar{x})-\varepsilon_{\mathrm{L}}\xi_{\mathrm{S}}(\bar{x})\}\frac{\mathrm{d}}{\mathrm{d}\varepsilon}\{D(\xi(\bar{x}+\varepsilon u))\}|_{\varepsilon=0}$$

$$-\varepsilon_{\mathrm{L}}D(\xi(\bar{x}))\frac{\mathrm{d}}{\mathrm{d}\varepsilon}\{\xi_{\mathrm{S}}(\bar{x}+\varepsilon u)\}|_{\varepsilon=0}+D(\xi(\bar{x}))\frac{\mathrm{d}}{\mathrm{d}\varepsilon}\{E(\bar{x}+\varepsilon u)\}|_{\varepsilon=0}. \tag{17}$$

The contributions from the first three terms in eqn (17) are considered separately here and, moreover, the first two terms must be considered individually for each of the separate regions of martensite or austenite transformation as delineated in eqns (6) and (7).

The third expression of eqn (17) simply requires the linearization of the Green strain. In the one-dimensional case of the truss element, the component in the direction of the material, E, is calculated from the displacements u, v and w as

$$E = u_{,x}+\tfrac{1}{2}(u_{,x}^2+v_{,x}^2+w_{,x}^2), \tag{18}$$

where commas represent differentiation. The linearization at a known configuration, $\bar{x}$, with corresponding displacements $\bar{u}$, $\bar{v}$, $\bar{w}$ reads

$$\frac{\mathrm{d}}{\mathrm{d}\varepsilon}\{E(\bar{x}+\varepsilon u)\}|_{\varepsilon=0} = (1+\bar{u}_{,x})u_{,x}+\bar{v}_{,x}v_{,x}+\bar{w}_{,x}w_{,x}. \tag{19}$$

In view of the finite element formulation, this equation can be written in vector notation as

$$\frac{\mathrm{d}}{\mathrm{d}\varepsilon}\{E(\bar{x}+\varepsilon u)\}|_{\varepsilon=0} = \bar{\mathbf{F}}^{\mathrm{T}}\cdot\mathrm{grad}\,\mathbf{u}, \tag{20}$$

defining the deformation gradient $\bar{\mathbf{F}}$ at the known configuration, $\bar{x}$, and the displacement gradient, grad $\mathbf{u}$, by

$$\bar{\mathbf{F}} = \begin{Bmatrix} 1+\bar{u}_{,x} \\ \bar{v}_{,x} \\ \bar{w}_{,x} \end{Bmatrix}, \quad \mathrm{grad}\,\mathbf{u} = \begin{Bmatrix} u_{,x} \\ v_{,x} \\ w_{,x} \end{Bmatrix}. \tag{21}$$

Returning to (17), consider first the transformation of martensite to austenite, where the relationship between stress and the martensite fraction is given by eqns (7a)–(7c). In this case the derivative in the second term in (17) can be written as

$$\frac{\mathrm{d}}{\mathrm{d}\varepsilon}\{\xi_S(\bar{x}+\varepsilon u)\}|_{\varepsilon=0} = \frac{\mathrm{d}}{\mathrm{d}\varepsilon}\left\{\xi_{S0}-\frac{\xi_{S0}}{\xi_0}(\xi_0-\xi(\bar{x}+\varepsilon u))\right\}\Bigg|_{\varepsilon=0}$$

$$= \frac{\xi_{S0}}{2}\frac{\mathrm{d}}{\mathrm{d}\varepsilon}\left\{\cos\left[a_A\left(T-A_s-\frac{S}{C_A}\right)\right]+1\right\}\Bigg|_{\varepsilon=0}. \tag{22}$$

Solving further and isolating the directional derivative of S, one finds

$$\frac{\mathrm{d}}{\mathrm{d}\varepsilon}\{\xi_S(\bar{x}+\varepsilon u)\}|_{\varepsilon=0} = \frac{\xi_{S0}}{2}\frac{a_A}{C_A}\sin\left[a_A\left(T-A_s-\frac{\bar{S}}{C_A}\right)\right]\frac{\mathrm{d}}{\mathrm{d}\varepsilon}\{S(\bar{x}+\varepsilon u)\}|_{\varepsilon=0}, \tag{23}$$

where $\bar{S}$ is the value of the function S at $\bar{x}$ and in general for subsequent expressions the shorthand notation of an overbar is used to represent the value of the variable at $\bar{x}$. In the first term in (17), the derivative may be expressed again as a derivative of the martensite fraction

$$\frac{\mathrm{d}}{\mathrm{d}\varepsilon}\{D(\xi(\bar{x}+\varepsilon u))\}|_{\varepsilon=0} = \frac{\mathrm{d}}{\mathrm{d}\varepsilon}\{D_a+(D_m-D_a)\xi(\bar{x}+\varepsilon u)\}|_{\varepsilon=0}$$

$$= (D_m-D_a)\frac{\xi_0}{2}\frac{\mathrm{d}}{\mathrm{d}\varepsilon}\left\{\cos\left[a_A\left(T-A_s-\frac{S}{C_A}\right)\right]+1\right\}\Bigg|_{\varepsilon=0}. \tag{24}$$

And using the same procedure as applied to the first term produces

$$\frac{\mathrm{d}}{\mathrm{d}\varepsilon}\{D(\xi(\bar{x}+\varepsilon u))\}|_{\varepsilon=0}$$

$$= (D_m-D_a)\frac{\xi_0}{2}\frac{a_A}{C_A}\sin\left[a_A\left(T-A_s-\frac{\bar{S}}{C_A}\right)\right]\cdot\frac{\mathrm{d}}{\mathrm{d}\varepsilon}\{S(\bar{x}+\varepsilon u)\}|_{\varepsilon=0}. \tag{25}$$

Returning to (17) and collecting terms from eqns (20), (23) and (25), the entire expression may be written for the case of transformation to austenite as

$$\frac{\mathrm{d}}{\mathrm{d}\varepsilon}\{S(\bar{x}+\varepsilon u)\}|_{\varepsilon=0} = \{\bar{E}-\varepsilon_L\bar{\xi}_S\}(D_m-D_a)\frac{\xi_0}{2}\frac{a_A}{C_A}\sin\left[a_A\left(T-A_s-\frac{\bar{S}}{C_A}\right)\right]$$

$$\times\frac{\mathrm{d}}{\mathrm{d}\varepsilon}\{S(\bar{x}+\varepsilon u)\}|_{\varepsilon=0}-\varepsilon_L\bar{D}\frac{\xi_{S0}}{2}\frac{a_A}{C_A}\sin\left[a_A\left(T-A_s-\frac{\bar{S}}{C_A}\right)\right]$$

$$\times\frac{\mathrm{d}}{\mathrm{d}\varepsilon}\{S(\bar{x}+\varepsilon u)\}|_{\varepsilon=0}+\bar{D}\bar{\mathbf{F}}^{\mathrm{T}}\cdot\mathrm{grad}\,\mathbf{u}. \tag{26}$$

Utilizing the recursive relationship apparent in this expression, rearranging and solving, one obtains a closed form expression for the linearized shape memory alloy constitutive law in the case of transformation of martensite to austenite as desired:

$$\frac{\mathrm{d}}{\mathrm{d}\varepsilon}\{S(\bar{x}+\varepsilon u)\}|_{\varepsilon=0} = \frac{1}{(1-H_1H_2)}\bar{D}\bar{\mathbf{F}}^{\mathrm{T}}\cdot\mathrm{grad}\,\mathbf{u}, \tag{27}$$

where H_1 and H_2 are defined as

$$H_1 = \frac{a_A}{C_A}\sin\left[a_A\left(T - A_s - \frac{\bar{S}}{C_A}\right)\right],$$

$$H_2 = (\bar{E} - \varepsilon_L\bar{\xi}_S)(D_m - D_a)\frac{\xi_0}{2} - \varepsilon_L\bar{D}\frac{\xi_{S0}}{2}. \tag{28}$$

Similarly, for the case of transformation to detwinned martensite for temperatures greater than martensite start, eqns (6a) and (6b) can be used in conjunction with eqn (17) to obtain

$$\frac{d}{d\varepsilon}\{S(\bar{x}+\varepsilon u)\}|_{\varepsilon=0} = \frac{1}{(1-H_3H_4-H_3H_5)}\bar{D}\bar{\mathbf{F}}^T\cdot\text{grad}\,\mathbf{u}, \tag{29}$$

where H_3, H_4 and H_5 are defined as

$$H_3 = -\frac{\pi}{\sigma_s^{cr}-\sigma_f^{cr}}\sin\left[\frac{\pi}{\sigma_s^{cr}-\sigma_f^{cr}}(\bar{S}-\sigma_f^{cr}-C_M(T-M_s))\right],$$

$$H_4 = (\bar{E}-\varepsilon_L\bar{\xi}_S)(D_m-D_a)\left(1-\frac{\xi_{T0}}{1-\xi_{S0}}\right)\frac{1-\xi_{S0}}{2},$$

$$H_5 = -\varepsilon_L\bar{D}\frac{1-\xi_{S0}}{2}. \tag{30}$$

And finally, for the case of transformation to detwinned martensite for temperatures less than martensite start, eqns (6c)–(6e) can be used together with eqn (17) to obtain

$$\frac{d}{d\varepsilon}\{S(\bar{x}+\varepsilon u)\}|_{\varepsilon=0} = \frac{1}{(1-H_4H_6-H_5H_6)}\bar{D}\bar{\mathbf{F}}^T\cdot\text{grad}\,\mathbf{u}, \tag{31}$$

where H_4 and H_5 are the same expressions as above and H_6 is given by

$$H_6 = -\frac{\pi}{\sigma_s^{cr}-\sigma_f^{cr}}\sin\left[\frac{\pi}{\sigma_s^{cr}-\sigma_f^{cr}}(\bar{S}-\sigma_f^{cr})\right]. \tag{32}$$

Note that the equations generated for the derivative of the constitutive relation in each of the three different transformation cases differ from the traditional elasticity result only by the preceding multiplicative term involving the H_i variables ($i = 1,\ldots,6$). The H_i variables themselves are fortuitously functions only of material constants and the value of stress at $\bar{x}$, which is known for each iteration.

Finite element formulation

For the numerical solution of eqn (12) with the incorporated linearized second Piola–Kirchhoff stress [eqns (27), (29) or (31)] the finite element method is used. For two noded truss elements, the displacement field is calculated from the nodal displacements by the well known equations

$$u = \sum_{k=1}^{2} N_k u_k, \quad v = \sum_{k=1}^{2} N_k v_k, \quad w = \sum_{k=1}^{2} N_k w_k, \tag{33}$$

where N_k are linear shape functions and u_k, v_k, w_k represent the nodal displacement at node k. The displacement gradient defined in eqn (21) in vector notation is now expressed via the matrix $[B]$ which contains the derivatives of the shape functions

$$\begin{Bmatrix} u_{,x} \\ v_{,x} \\ w_{,x} \end{Bmatrix} = \begin{bmatrix} N_{1,x} & 0 & 0 & N_{2,x} & 0 & 0 \\ 0 & N_{1,x} & 0 & 0 & N_{2,x} & 0 \\ 0 & 0 & N_{1,x} & 0 & 0 & N_{2,x} \end{bmatrix} \begin{Bmatrix} u_1 \\ v_1 \\ w_1 \\ u_2 \\ v_2 \\ w_2 \end{Bmatrix}. \tag{34}$$

Equations (12) and (13) and one of the equations (27), (29) or (31) are combined and cast into a notation appropriate to form the nonlinear element stiffness matrix for shape memory alloy material behavior

$$[K]^e = H\bar{D}A \int_l [B]^T \mathbf{F}\mathbf{F}^T [B]\, dx + \bar{S}A \int_l [B]^T [B]\, dx, \tag{35}$$

where A and l are the cross-sectional area and the length of the truss member, $\mathbf{F}$ is defined by eqn (21) and H represents the multiplicative factor dependent upon the H_i variables for each of the three transformation cases delineated in eqns (27), (29) and (31). For the case of martensite to austenite conversion, for example, (35) becomes

$$[K]^e = \frac{1}{(1-H_1 H_2)} \bar{D}A \int_l [B]^T \mathbf{F}\mathbf{F}^T [B]\, dx + \bar{S}A \int_l [B]^T [B]\, dx. \tag{36}$$

The other two cases for transformation to detwinned martensite are identical to (36) with the substitution of the corresponding multiplicative fraction containing the H_i variables. Note that the formulation in eqn (35) differs from the standard finite element formulation for nonlinear truss members only by this H factor. It should be emphasized that the H factor preserves quadratic convergence in a solution algorithm based on Newton's method and that eqn (35) represents the exact tangent modulus of the underlying problem.

In the following analyses presented, the Finite Element Analysis Program (FEAP), developed originally by Taylor (Taylor, 1982; Zienkiewicz and Taylor, 1989) was chosen for use in this study because of its segmented structure, which allows relatively easy modification of the subroutines without requiring interdependent changes scattered throughout the entire program. In order to address shape memory alloy problems, the code's element subroutine was revised to calculate a nonlinear elasticity truss element, as developed in the previous subsection. At each iteration of the nonlinear analysis, the prediction for the Green strain from the previous step, $\bar{E}$, was utilized to calculate the corresponding value of $\bar{S}$. Due to the coupled nature of the SMA constitutive equations, this task was accomplished by the addition of an iterative subroutine which separately calculates the values and contributions of the martensite internal variables to the stress value, given the strain and temperature from the element subroutine. Equations (5)–(7) are entirely embedded in this additional procedure and are external to the original finite element routines. Note that if the value of stress, $\bar{S}$, from this subroutine and temperature are such that the material is not in a transformation region, then the multiplicative H factor reduces identically to 1 and the nonlinear elasticity formulation is left unmodified.

DISCUSSION AND APPLICATIONS

A finite element procedure was modified as indicated in the previous section and then utilized to calculate the responses of shape memory alloy elements both alone and as parts of other structures. There are several points for caution in the use of such a numerical procedure for problems containing shape memory alloys. First note that the transformation equations describing the relationship between martensite fraction, temperature and stress and the assumption that the material parameters are linearly dependent upon ξ, although

Table 1. Material properties for the Nitinol alloy used in the examples (Dye, 1990; Liang, 1990)

Moduli, density	Transformation temperatures	Transformation constants	Maximum residual strain
$D_a = 67 \times 10^3$ MPa	$M_f = 9°C$	$C_M = 8$ MPa °C^{-1}	$\varepsilon_L = 0.067$
$D_M = 26.3 \times 10^3$ MPa	$M_s = 18.4°C$	$C_A = 13.8$ MPa °C^{-1}	
$\Theta = 0.55$ MPa °C^{-1}	$A_s = 34.5°C$	$\sigma_s^{cr} = 100$ MPa	
$\rho = 6448.1$ kg m^{-3}	$A_f = 49°C$	$\sigma_f^{cr} = 170$ MPa	

generally accurate in nature for a wide variety of shape memory alloys, might need modification to obtain the most accurate results with some particular alloy. In this case, the procedure outlined in this paper and previously (Brinson, 1993) would need to be followed to modify the governing equations of the material system and for the numerical procedure. However, for most alloys and applications, careful testing to obtain the variety of material parameters should be sufficient to characterize the material for use with the equations developed here. The most crucial parameters are the ones appearing in the critical transformation stress curves.

It should also be noted that the examples given here utilize existing experimental data on noncycled specimens. For most shape memory alloys the appearance of the curves in Fig. 2 and likewise the material parameters change with repeated cyclic loading of the material, stabilizing after as few as 20–30 cycles. In general, the transformation region itself becomes very narrow as the specimen is essentially "trained" to perform a particular transformation repeatedly. However, in many cases, if a cycled specimen is heated stress-free well above the A_f temperature and retested, then the behavior returns to that of an uncycled specimen. Unfortunately, to date there is no consistent data or mathematical description to portray the transition between uncycled and cyclic behavior. Consequently, the data for either cycled or uncycled specimens must be chosen as is most appropriate to the application being modeled. As an added note on the critical transformation stresses, there is evidence that the precise path of the stress–strain hysteresis evolves under partial loading and unloading situations (partial transformations) as a function of return points. Although the character of the hysteresis and magnitudes of the stresses and strains achieved remains the same as described by eqns (6) and (7), if the exact path is of importance in a particular application, additional expressions such as those under investigation by Ortín (1991) should be employed in conjunction with the expressions given here.

In the finite element implementation itself, one must be certain that the reference state, or initial conditions of the material ($S_0, E_0, \xi_0, \xi_{S0}, T_0$), are sensible—that they represent a possible state of existence for the shape memory alloy. If this is not the case, the numerics will either be unable to converge on a solution or will yield misleading results.

Abiding by the preceding requirements and caveats, the finite element procedure developed for study of shape memory alloy behavior presents us with a very powerful tool for investigating current and potential applications which utilize the unique capabilities of SMAs to produce large strains or stresses under temperature change. In the following, several test cases will be examined: first, the one-dimensional behavior of a SMA material alone, followed by two successively more complex applications. The material properties for the shape memory alloy in the following examples are taken from data given by Dye (1990) and Liang (1990) on a nitinol alloy ($Ni_{55}Ti$). The values for the necessary material properties are listed in Table 1.

Simple one-dimensional SMA behavior

In order to perform the most basic test on the finite element procedure developed and in order to present a basis for the subsequent applications of SMAs, two simple one-dimensional tests illustrating the thermomechanical response of SMAs are performed in this section: stress–strain behavior at various temperatures and restrained recovery.

The stress–strain responses for a wide range of temperatures are shown in Fig. 3. For all of these curves, the initial value of the stress-induced martensite variable is clearly zero

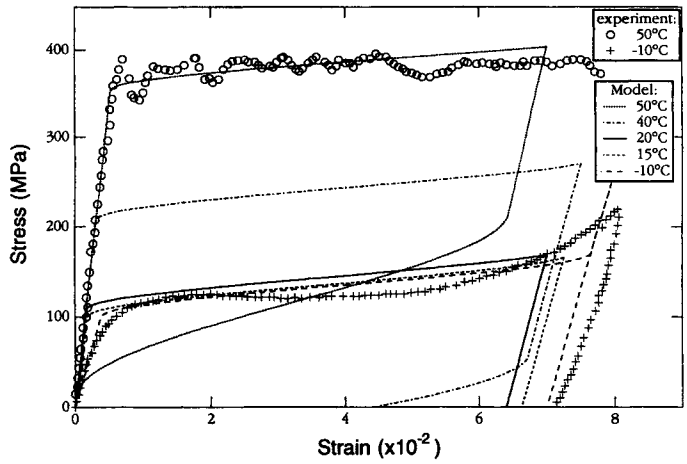

Fig. 3. SMA stress–strain curves calculated by the finite element procedure illustrating the pseudoelastic effect and the shape memory effect. $\xi_{S0} = 0$ in all cases ($A_s = 34.5°C$). Experimental data from Liang (1990).

as indicated by lack of residual initial strain. For temperatures above M_s, the initial value of the temperature-induced martensite variable was taken to be zero and for temperatures less than M_s, the initial values of ξ_T were proportional to temperature as indicated by eqn (6e). With these initial conditions, only the curve for $T = -10°C$ is representative of a fully martensitic specimen before loading. At $T = 15°C$ the material is partially martensite and partially austenite prior to application of stress and at all higher temperatures the material is fully austenite. The subsequent different initial values of the modulus functions are manifested in the difference in slope of the linear loading portion of the stress–strain curves. Experimental results from Liang (1990) are given for the loading curve of 50°C† and the loading and unloading curves of $-10°C$. The agreement between the experiment and the model is quite good.

The stress–strain responses at temperatures less than austenite start are all indicative of the shape memory effect: The material loads elastically, then undergoes conversion of martensite variants and/or transformation of austenite to detwinned martensite during the nonlinear portion of the stress–strain curve, and finally unloads elastically (with no pseudoelastic recovery) incurring a residual strain. To complete the shape memory effect for the curves at temperatures below A_s, the material temperature must be raised above the austenite finish temperature at zero stress for the material to recover all of the residual strain. The pseudoelastic effect is demonstrated in Fig. 3 by the curves for $T = 40°C$ and $T = 50°C$. Since the lower of these two temperatures is less than A_f, there is only a partial pseudoelastic strain recovery on unloading and the material consists of both detwinned martensite and austenite after unloading. At $T = 50°C$, above A_f, the material exhibits a complete hysteresis loop during the procedure: The material is austenite prior to loading, transforms to detwinned martensite during loading and completes the inverse transformation to austenite upon unloading.

Note that the curves in Fig. 3 are identical to the analytical results presented for these cases elsewhere (Brinson, 1993), in which eqns (5)–(7) are used to solve directly for the stress–strain behavior at the different temperatures. To obtain such results for SMA mechanical behavior, the stress history must be considered. Therefore, the finite element procedure is first applied with incremental values of load and the initial conditions of the origin; then the values of the variables at the end of loading are taken as initial conditions and the load is decremented.

†The experiment for 50°C unfortunately delved into the irrecoverable plasticity range, thus the unloading curve is not given. Other experimental works clearly show the pseudoelastic effect of unloading at $T > A_f$ and agree very well with the results shown here.

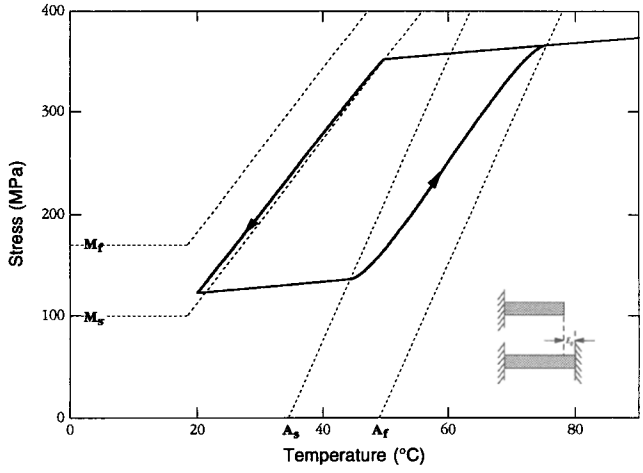

Fig. 4. Restrained recovery with $E_0 = 0.5\%$, $\xi_{S0} = 0.046$, $\xi_{T0} = 0$, $S_0 = 128$ MPa. Curves of critical stress for transformation also shown.

In the case of restrained recovery, a material with residual strain is constrained to maintain that deformation as the temperature is raised through A_s and A_f. Figure 4 shows a material with 0.5% residual strain subjected to these conditions ($E = E_0 = 0.005$). Because the material is restrained as the inverse transformation to austenite occurs, and the material would recover the residual strain if unrestrained, extremely large internal stresses are incurred. Figure 4 also shows the critical transformation stress curves for ease of comparison. It is clear that upon heating the internal stress increases rapidly during transformation to austenite, after transformation is complete the stress remains essentially constant, and as the specimen is cooled the internal stress decreases rapidly in the region of the austenite to martensite transformation. Note that the hysteresis loop here starts and ends with a definite value of stress; this value is the amount of stress required at $T = 20°C$ to achieve a 0.005 strain.

It is important to note that these results agree extremely well both quantitatively and qualitatively with experimental data on SMA materials. In the case of restrained recovery, however, note that experimental measurements are generally performed with at least 0.01 or 0.02 residual strain (detwinned martensite), which is far too large to expect that the material could attain 100% austenite conversion without encountering plasticity. Consequently, for accurate calculation of the maximum stress achieved in restrained recovery, experimental data on the critical plastic stress limits for SMAs must be used so that once the plasticity region is entered, the numerical procedure halts the transformation.

SMA pipe coupling

One of the most established uses for shape memory alloys is that of connectors for tubing and, similarly, pin and socket type connectors (Harrison and Hodgson, 1976). The procedure in these applications is to manufacture a ring of shape memory alloy that has a somewhat smaller inner diameter in the austenitic state than the outer diameter of the pipes to be connected. At a temperature less than A_s the ring is then deformed into partially detwinned martensite such that its inner diameter exceeds slightly that of the tubing. The ring is placed over the pipes in this phase and then heated. As the transformation to austenite takes place, the material attempts to recover the initial residual strain. Being partially constrained, however, by the strength of the pipe material, the SMA ring subsequently recovers only part of its residual strain and as a result builds up large internal stresses; both of these effects together superbly seal the connection. In practice, the martensite temperatures are generally chosen to be well below the operating temperatures so that the SMA ring is deformed and stored at very low temperatures; then when applied quickly to connect the pipes, the seal is immediately effected as the material warms up to the ambient temperature.

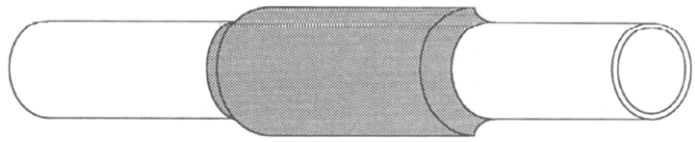

Fig. 5. Schematic of pipes or tubing connected by a shape memory alloy ring.

In this section, two analyses are undertaken to simulate this application (Fig. 5) and to demonstrate the accuracy of the finite element calculation with respect to analytical results. The finite element procedure is utilized with two one-dimensional rings of truss elements linked together at the nodes: one ring of elements is of the shape memory alloy, the other is of the pipe material [Fig. 6(a)]. The shape memory alloy is given an initial strain of 0.02 in the θ-direction at $T_0 = 20°C$ ($\xi_{S0} = E_0/\varepsilon_L$) and then the structure is heated to various temperatures and the resulting stresses and strains calculated. The second analysis is a two-dimensional superposition problem, considering the cross-sections of the tubing and the SMA ring [Fig. 6(b)], which is solved analytically for the stresses and strains at the interface and compared to the finite element results. The standard equations for elasticity of hollow circular domains and the interface fit superposition technique as found in Timoshenko and Goodier (1970) are utilized here; for the ring of SMA material the constitutive relation is of necessity modified. The assumption is made that the shape memory alloy only has residual strain activated in the θ-direction (reasonable for actual applications) and that consequently the behavior in the radial direction is elastic in nature. With these assumptions, the results for the stresses and strains in the radial and θ-directions were calculated.

Schematics of the one-dimensional and two-dimensional domains studied are shown in Figs 6(a) and 6(b) and the stress and strain results comparing the numerical and analytical solutions are given in Figs 7–9. The values shown for the strain are the differences from the original E_0 value. Note that the values calculated for the radial stress in the two-dimensional problem are several orders of magnitude smaller than the stress which develops in the θ-direction at any temperature, thus justifying the essentially one-dimensional nature of this

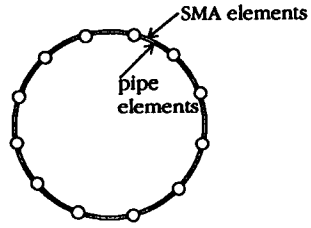

Fig. 6(a). One-dimensional finite element approximation of SMA coupling for pipes.

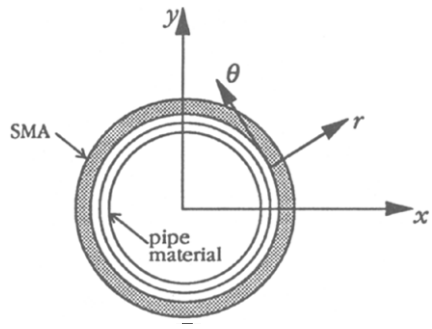

Fig. 6(b). Two-dimensional analytical approximation of SMA coupling for pipes, solved by superposition.

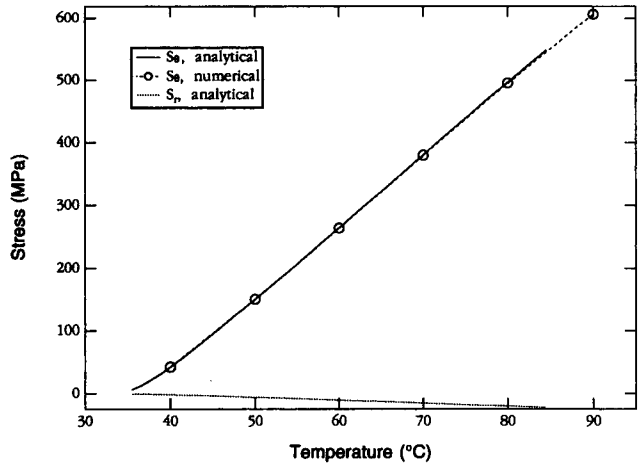

Fig. 7. Comparison of analytical and numerical results for the interface stresses as functions of temperature in a pipe coupling via a SMA ring. $D_{pipe} = 65 \times 10^3$ MPa.

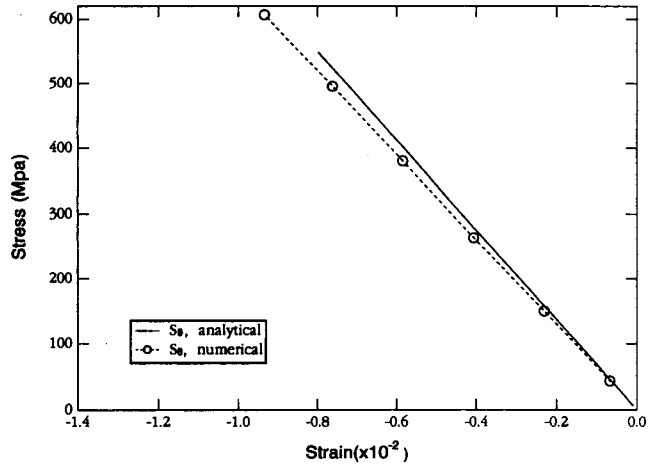

Fig. 8. Comparison of analytical and numerical results for the stress and strain at the interface in a pipe coupling via a SMA ring. $D_{pipe} = 65 \times 10^3$ MPa.

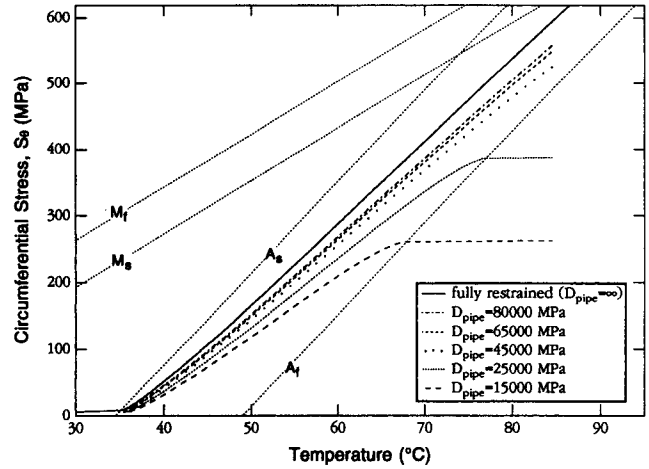

Fig. 9. Results for the circumferential interface stresses as functions of temperature in a pipe coupling via a SMA ring with various values of the Young's modulus for the pipe, D_{pipe}. Transformation regions for the shape memory alloy are also shown. (For comparison, note that for the SMA material: $D_a = 67{,}000$ MPa, $D_m = 26{,}000$ MPa.)

problem.† Generally, it can be assumed that a one-dimensional theory is sufficient for a thin walled ring: Thickness of the SMA coupler less than 5% of its diameter. The results presented here for the two-dimensional analysis are for equal thicknesses of the shape memory ring and the two pipes together, and for a thickness/diameter ratio of 0.02 for the SMA. If the pipe to be sealed has, for example, walls of twice the thickness of the SMA ring, then this is identical to the effect of doubling the modulus of the pipe material in the one-dimensional finite element analysis. Thus, using physical insight into the problem allows a purely one-dimensional finite element study to be used effectively in examining this two-dimensional problem.

This example was chosen to establish the accuracy of the finite element compared to analytical results, even though in the one-dimensional case a lumped parameter model could be used to calculate the results as well, in place of the finite element formulation. A finite element analysis of the pipe coupling problem could also be performed using two-dimensional shell elements for the pipe linked with truss elements for the SMA, as illustrated for a different example in the following section. This formulation would lead to more accurate results and yield profiles of the critical parameters throughout the cross-section of the pipe, which could not be accomplished by a simple lumped-parameter model.

The results of the stresses at the SMA–pipe interface are shown for a variety of strengths of the pipe material in Fig. 9, with the Young's modulus spanning from values lower than the martensitic modulus of the SMA to values exceeding the austenitic modulus. In the latter case, it is clear that the results are converging on the case of pure restrained-recovery (infinite modulus for the pipe material) as one would expect. The depiction of the critical stress curves for the SMA material itself in Fig. 9 demonstrates the location in the transformation region at any particular point. Such a diagram could be well used to mark off the operating temperatures of the component and the maximum stress desired at the interface to bound the regions of interest. Then different values of initial strain and alloys with slightly differing material parameters could be studied with the finite element procedure to determine the optimal material for the operating constraints of the part in question.

Active frequency tuning of a composite strip

One reason for the growing interest in shape memory alloys in recent years is due to the fact that SMAs are candidate materials for smart structure applications. With integrated actuators and sensors, smart, adaptive or intelligent structures allow for vibration control, shape control, alignment precision control and damage detection (Breitbach, 1991). The remarkable features of SMAs that make them especially suitable for active elements in actuators are their capacity for high forces, high displacements, reliability with temperature control and potential to create compact powerful actuators. Moreover, in contrast to actuators based on piezoelectric or magnetostrictive materials, SMA-actuators offer the advantage that they can exert large repeatable displacements at zero or constant load. Although for some devices their use is limited by the low frequency (maximum 2 Hz) at which they can be run, nevertheless SMAs can be used in many dynamic applications. One possibility currently being researched is structures with embedded wires of shape memory material, activated by an electrical current to vary the temperature. In this manner internal stress states are created in the structure that influence the eigenfrequencies. Active frequency tuning of this type can be used, for example, to avoid resonances. An investigation of this particular application of SMAs is demonstrated by the finite element procedure in the following example.

Figure 10 shows a fiber-reinforced composite strip with eight embedded SMA wires. The material properties of the composite strip are given in Table 2, while those of the SMA wires are taken from Table 1. The structure with a total length of 1 m is clamped at both ends. The initial conditions are a 0.5% residual strain of the SMA wires, no prestress and

†Note that although there is discrepancy between the Cauchy and Second Piola–Kirchhoff stresses utilized for the different constitutive laws in this analysis, the effects at the strain levels achieved here are so minor as to be negligible.

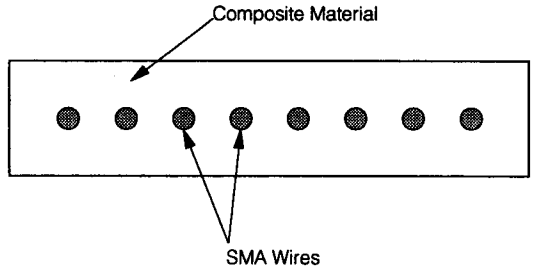

Fig. 10. Cross-section of composite strip with embedded SMA wires in active frequency tuning example. Diameter of wires is taken to be 0.5 mm.

temperature $T_0 = 20°C$. From these values the stress-induced and temperature-induced martensite fractions are calculated as $\xi_{S0} = 0.075$ and $\xi_{T0} = 0$, respectively.

In the numerical experiment the first two eigenfrequencies of this structure are calculated as a function of temperature. The results are presented in Fig. 11. When the structure is heated there is a slight decrease in the eigenfrequencies until the temperature reaches 35°C. In the range from 35°C to 75°C there is a strong increase in the eigenfrequencies after which they slowly decrease again when the temperature exceeds 75°C. When the structure is cooled a hysteresis loop of the eigenfrequency versus temperature curve is observed. Note that the frequency at the end of the cooling cycle does not return to pre-loading levels; this is due to the fact that because of the high stresses obtained during heating, upon cooling the material first encounters the state at which that stress level and the T_0 temperature would produce a strain of 0.005 in the shape memory alloy. As the specimen is heated again from here, one obtains the closed hysteresis cycle. To obtain the original values of the frequencies, the material must be unclamped and the residual stress removed from the shape memory wires.

Since the eigenfrequencies depend strongly on the axial force of this structural system, the behavior is explained by comparison of Fig. 4 and Fig. 11. In the case of restrained recovery, the stress due to heating rises primarily within the temperature range 35–75°C (the region of martensite to austenite transformation) and, therefore, the change of the eigenfrequencies in the clamped strip reflects this behavior. The slight decrease of the eigenfrequencies with increasing temperature from 20 to 35°C and above 75°C is explained by the compression force exerted by the composite strip (due to constraint of the normal thermal expansion) and cannot be compensated for by the SMA wires outside of the transformation region. The hysteresis loop seen upon cooling is due to the shape memory behavior for the inverse transformation to martensite as in the case of restrained recovery. These results for the change in eigenfrequencies of a fiber-reinforced composite strip with embedded SMA wires agree well qualitatively with experimental results on a similar system studied by Mooi (1992). Direct comparison of numerical results is not possible due to the lack of detailed information on the material properties in the experiments.

The numerical results were obtained by discretization of the structural system by both SMA truss finite elements and non-linear beam elements. Linking the corresponding nodes has the effect that the stiffness and mass matrices of the SMA truss elements and composite beam elements are added. Note that in this technique only the composite strip contributes to the bending stiffness of the system and that the axial forces of both the composite strip

Table 2. Material properties for the fiber-reinforced composite used in the examples

Tension stiffness	$DA = 3.050 \times 10^{-5}$ N
Bending stiffness	$DI = 2.074$ N m^2
Mass per length	$\mu = 3.5 \times 10^{-2}$ kg m^{-1}
Thermal coefficient of expansion	$\alpha = 1.2 \times 10^{-6}$ °C^{-1}

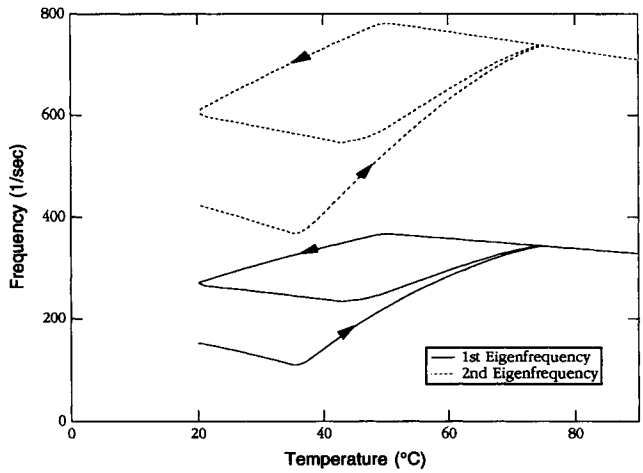

Fig. 11. Variance of eigenfrequencies of composite beam with temperature. For embedded SMA wires $E_0 = 0.005$.

and the SMA wires are accounted for. Using one-dimensional truss elements to represent SMA wires in structures, many more complex situations can be analysed with the finite element technique by the procedure described here. Such analyses will be the subject of future papers.

CONCLUSION

Here we have developed and demonstrated a nonlinear finite element procedure for one-dimensional shape memory alloy behavior. The constitutive law chosen for this work is one that accurately predicts the behavior of a wide variety of SMAs and utilizes only easily quantifiable material parameters. Due to the nature of their internal crystalline transformations which accommodate extremely large reversible strains, shape memory alloys are often best utilized in components that are subject to or activate mechanical forces restricted to one dimension. Consequently the finite element equations were developed for a one-dimensional truss system.

The constitutive equations for SMA behavior were encapsulated into an iterative subroutine external to a nonlinear elasticity element routine. The SMA constitutive law is of such a form that its linearization for use in the Newton's method finite element solution resulted in contained factors clearly separable in the elasticity formulation. One consequence of this direct implementation is that in the eventual case of modification of the SMA constitutive law to deal with unusual shape memory behavior, necessary changes to the external SMA subroutine and the derivative factors can be made relatively easily and quickly. Considerations that would necessitate modification of the basic SMA constitutive relations would be the use of a shape memory material with more complex functionality of the material parameters with the independent variables than is presented here.

The finite element procedure for shape memory alloy truss elements provides a powerful tool to study SMA components in various applications, as illustrated by several examples in this paper. The one-dimensional functionality of a SMA component can be studied alone, subject to boundary conditions imposed by the system, or entire composite systems can be studied. In the analysis of composite systems, either the entire system can be reduced to an equivalent one-dimensional problem or, more importantly, the SMA components can be represented by truss elements linked to the two-dimensional structure in the finite element analysis.

With an eye toward future developments in this area, careful experimental characterization of shape memory alloy behavior in two dimensions subject to multiaxial loading and subsequent development of an accurate multi-dimensional constitutive law would allow even more precise numerical studies of current SMA devices and perhaps give insight into new applications in which SMAs could be useful even if not utilized in an entirely one-

dimensional manner. Also, the finite element procedure itself, as it stands now, could benefit from the addition of heat transfer effects to the derivation technique in order to consider an even wider variety of applications.

Acknowledgements—The authors wish to gratefully acknowledge the Deutsche Forschungsanstalt für Luft- und Raumfahrt and the American Association for University Women Educational Foundation for supplying the resources and the funding with which this work was completed.

REFERENCES

Achenbach, M. (1989). A model for an alloy with shape memory. *Int. J. Plast.* **5,** 371–395.

Banks, R. and Weres, O. (1976). *Shape Memory Effects in Alloys*. Plenum Press, New York.

Breitbach, E. (1991). Research status on adaptive structures in Europe. *2nd Joint Japan/US Conference on Adaptive Structures*, Nagoya, Japan, 12–14 November. Technomic Publishing, Lancaster.

Brinson, L. C. (1992). Constitutive behavior of shape memory alloys: one dimensional thermomechanical derivation with non-constant material functions and redefined martensite internal variable. *Conference on Recent Advances in Adaptive and Sensory Materials and their Applications*, Virginia Tech, Blacksburg, VA, 27–29 April. Technomic Publishing, New York.

Brinson, L. C. (1993). One dimensional constitutive behavior of shape memory alloys: thermomechanical derivation with non-constant material functions. *J. Intelligent Material Systems & Structures* **4**(2), 229–242.

Delaey, L., Krishnan, R. V., Tas, H. and Warlimont, H. (1974). Review—Thermoelasticity, pseudoelasticity and the memory effects associated with martensitic transformations—Part 2: The macroscopic mechanical behavior. *J. Mater. Sci.* **9,** 1536–1544.

Dye, T. E. (1990). An experimental investigation of the behavior of nitinol. MS Thesis, Virginia Tech.

Falcioni, J. G. (1992). Shape memory alloys. *Mech. Engng* **114**(4).

Falk, F. (1980). Model free energy, mechanics, and thermodynamics of shape memory alloys. *Acta Metal.* **28,** 1773–1780.

Falk, F. (1983). One-dimensional model of shape memory alloys. *Arch. Mech.* **35** (Warszawa), 63–84.

Funakubo, H. (1987). *Shape Memory Alloys* (translated from the Japanese by J. B. Kennedy). Gordon and Breach Science Publishers, New York.

Harrison, J. D. and Hodgson, D. E. (1976). Use of TiNi in mechanical and electrical connectors. In *Shape Memory Effects in Alloys* (Edited by J. Perkins). Plenum Press, New York.

Hughes, T. J. R. and Pister, K. S. (1978). Consistent linearization in mechanics of solids and structures. *Comput. Struct.* **8,** 391–397.

Liang, C. (1990). The constitutive modeling of shape memory alloys. PhD Thesis, Virginia Tech.

Liang, C. and Rogers, C. A. (1990). One-dimensional thermomechanical constitutive relations for shape memory materials. *J. Intell. Mater. Syst. Struct.* **1**(2), 207–234.

Marsden, J. E. and Hughes, T. R. J. (1983). *Mathematical Foundations of Elasticity*. Prentice-Hall, Englewood Cliffs.

McNichols, J. L. J. and Cory, J. S. (1987). Thermodynamics of nitinol. *J. Appl. Phys.* **61**(3), 972–984.

Mooi, H. G. (1992). Active control of structural parameters of a composite strip using embedded shape memory alloy wires. Diplomarbeit, University of Twente, the Netherlands and Deutsche Forschungsanstalt für Luft- und Raumfahrt, Göttingen, Germany.

Ortín, J. (1991). Partial hysteresis cycles in shape-memory alloys: experiments and modelling. *J. Physique* **IV,** C4-65–C4-70.

Perkins, J., Edwards, G. R., Such, C. R., Johnson, J. M. and Allen, R. R. (1976). Thermomechanical characteristics of alloys exhibiting martensitic thermoelasticity. In *Shape Memory Effects in Alloys* (Edited by J. Perkins). Plenum Press, New York.

Rogers, C. A., Liang, C. and Jia, J. (1989). Behavior of shape memory alloy reinforced composite plates—Parts I and II. In *Proceedings of the 30th Structures, Structural Dynamics and Materials Conference*, Mobile, Alabama, 3–5 April, pp. 2011–2017.

Tanaka, K. (1986). A thermomechanical sketch of shape memory effect: One dimensional tensile behavior. *Res. Mech.* **18,** 251–263.

Tanaka, K. and Iwasaki, R. (1985). A phenomenological theory of transformation superplasticity. *Engng Fract. Mech.* **21**(4), 709–720.

Tanaka, K. and Nagaki, S. (1982). A thermomechanical description of materials with internal variables in the process of phase transitions. *Ing. Arch.* **51,** 287–299.

Taylor, R. L. (1982). FEAP—Finite Element Analysis Program. University of California at Berkeley.

Timoshenko, S. P. and Goodier, J. N. (1970). *Theory of Elasticity* (3rd Edn). McGraw-Hill, New York.

Warlimont, H., Delaey, L., Krishnan, R. V. and Tas, H. (1974). Review—Thermoelasticity, pseudoelasticity and the memory effects associated with martensitic transformations—Part 3: Thermodynamics and kinetics. *J. Mater. Sci.* **9,** 1545–1555.

Wayman, C. M. (1980). Some applications of shape-memory alloys. *J. Metals* **32,** 129–137.

Wayman, C. M. and Duerig, T. W. (1990). An introduction to martensite and shape memory. In *Engineering Aspects of Shape Memory Alloys* (Edited by T. W. Duerig, K. N. Melton, D. Stöckel and C. M. Wayman), pp. 3–20. Butterworth-Heinemann, Boston.

Wriggers, P. (1988). *Konsistente Linearisierungen in der Kontinuumsmechanik und ihre Andwendungen auf die Finite-Element-Methode*. Habilitationsschrift, Universistät Hannover.

Zienkiewicz, O. C. and Taylor, R. L. (1989). *The Finite Element Method. Vol. 1: Basic Formulations and Linear Problems* (4th Edn). McGraw-Hill, London.